CMS Physics Analysis Summary

Contact: cms-pag-conveners-top@cern.ch 2011/10/03

Measurement of the $t\bar{t}$ Pair Production Cross Section at $\sqrt{s} = 7$ TeV using b-quark Jet Identification Techniques in Lepton + Jet Events

The CMS Collaboration

Abstract

An updated measurement of the production cross section for $pp \to t\bar{t}$ at a center-of-mass energy of 7 TeV using data collected by the CMS detector at the Large Hadron Collider is presented. The analysis uses data corresponding to an integrated luminosity between 0.8 and 1.1 fb^{-1} using events with one isolated, high transverse momentum muon or electron, large missing transverse energy and hadronic jets. The $t\bar{t}$ content of the data has been enhanced by requiring the presence of at least one jet consistent with originating from a b-quark. The cross section is extracted with a profile likelihood method using a fit to the number of reconstructed jets, the number of b-tagged jets, and the secondary vertex mass distribution. The measured cross section is 164.4 ± 2.8 (stat.) ± 11.9 (syst.) ± 7.4 (lum.) pb and is consistent with higher order QCD calculations. We perform a cross check analysis, which compares favorably to the main result.

1 Introduction

The top quark was first observed in proton-antiproton collisions at $\sqrt{s} = 1.8\,\text{TeV}$ at the Fermilab Tevatron collider [1, 2]. Since then its properties have been studied by the Tevatron experiments and found to be in agreement with Standard Model (SM) [3] expectations. With the turn-on of the Large Hadron Collider (LHC) [4], SM predictions for top-quark pair production are now being tested in proton-proton collisions at significantly higher energies. This allows for extended studies of top quark properties and an increasingly precise determination of the top quark pair production cross section, a SM process which may be an important background for new physics in the LHC energy regime.

In the Standard Model the top quark decays almost 100% of the time via the weak process $t \to Wb$. This article focuses on $\mathrm{t\bar{t}}$ decays in which one of the two W bosons decays hadronically and the other decays leptonically, at leading order giving a final state containing a charged lepton, a neutrino and four jets, two of which are from b-quarks. Here, we focus on the muon + jets and electron + jets channels where we have used a secondary vertex reconstruction algorithm [5] to distinguish b-quark jets from non b-quark jets. We present results for the cross section for $pp \to t\bar{t}$ based on a data sample in the electron+jets (muon+jets) channel corresponding to an integrated luminosity of 804 (1087) pb^{-1} [6] recorded by the CMS experiment between March and July 2011.

This analysis note represents an update of an earlier analysis [7] based on $36\,\text{pb}^{-1}$. A salient feature of the analysis is the simultaneous determination of the top pair production cross section and the dominant systematic uncertainties in a combined fit, taking into account the correlations. The reference analysis, described in the following sections, is cross checked by a dedicated analysis, which extracts the cross section using a template fit to the invariant mass distribution of the system built from this b-jet associated to the leptonically decaying top quark and the muon, $\mu\mu j$, and described in detail in Section 5 of this note.

2 Signal and Background Modeling

The efficiency for selecting lepton+jets signal events is determined using a simulated $\mathrm{t\bar{t}}$ event sample assuming a top quark mass of $\mathrm{m}_t = 172.5$ GeV. The simulation of $\mathrm{t\bar{t}}$ events is performed using MADGRAPH [8] Monte Carlo generator, where the top quark pairs are generated accompanied by up to three additional hard jets. The parton configurations generated by MADGRAPH are processed with PYTHIA [9] to provide showering of the generated particles. The shower matching is done using the Kt-MLM prescription [8]. The generated events are then passed through the full CMS detector simulation based on GEANT4 [10].

The electro-weak production of single top quarks is considered a background process, and is simulated using POWHEG. The production of W/Z + jet events, where the vector bosons decay leptonically, have a similar signature to $\mathrm{t\bar{t}}$, and constitute the main backgrounds. These are simulated using MADGRAPH, with up to four jets with the matrix element (ME) description, as are photon+jet events which are a background for the electron+ jets channel. The W/Z + jet events are inclusive with respect to jet flavor. The bottom and charm components are separated from the light flavor (uds and gluon) components in the analysis by matching reconstructed jets to partons in the simulation. In addition, QCD multi-jets are also considered as a background and samples were produced using PYTHIA.

The background processes are normalized to next and next-to next-leading order cross sections calculations, as listed below, with an exception of QCD background, normalization of which is

obtained using the fit to the $\not\!\!E_{\mathrm{T}}$ distribution in data.

The next-to-leading order (NLO) top-quark pair production cross section has been calculated as $\sigma_{\mathrm{t\bar{t}}} = 157^{+23}_{-24}$ pb, using MCFM [11]. The uncertainty in the cross section includes the scale uncertainties, estimated by varying the factorization and renormalization scales by factor 2 and 0.5 around the dynamical scale choice of $(2m_t)^2 + (\sum p_T^{jet})^2$ with m_t = 172.5 GeV. The uncertainties from the parton distribution function (PDF) fits and the value of α_S are estimated following the procedures from the MSTW2008 [12], CTEQ6.6 [13], and NNPDF2.0 [14] sets. The uncertainties are then combined according to the PDF4LHC prescriptions [15].

Similarly, the t-channel single top NLO cross-section has been determined as $\sigma_t = 64.6^{+3.4}_{-3.2}$ pb using MCFM [11, 16–18]. The uncertainty is evaluated similarly as for top-quark pair production. The single top-quark associated production (tW) cross section has been set to $\sigma_{tW} = 15.7 \pm 1.2$ pb [19]. The s-channel single top NNLL cross-section has been determined as $\sigma_t = 4.6 \pm 0.06$ pb [20].

The inclusive NNLO cross section of the production of W bosons decaying into leptons has been determined as $\sigma_{W\to l\nu} = 31.3 \pm 1.6$ nb using FEWZ [21], setting renormalization and factorization scales (the so-called "Q^2" scale) to $(m_W)^2 + (\sum p_T^{jet})^2$ with $m_W = 80.398$ GeV. The uncertainty was determined in a similar way as for top-quark pair production. Finally, the Drell-Yan production cross section at NNLO has been calculated using FEWZ as $\sigma_{Z/\gamma^*\to ll}(m_{ll} > 50\,\mathrm{GeV}) = 3048 \pm 132$ pb, where m_{ll} is the invariant mass of two leptons from Z boson decay, and the scales were set using a mass term of $m_Z = 91.1876$ GeV.

3 Event Selection

The trigger providing the data samples used in this analysis requires the presence of at least one charged lepton, either an electron or a muon with a minimum requirement on the transverse momentum (p_T) of $p_T > p_T^{\min}$. To retain efficiency over the whole run range we selected a trigger with minimum transverse momentum $p_T^{\min}$ threshold of 30 GeV for muons, and ranging from 27 to 42 GeV for electrons. These triggers are nearly fully efficient above these thresholds. In addition, the electron trigger features an isolation requirement consistent with our offline selection in order to maintain a feasible trigger rate while keeping the kinematic thresholds as low as possible.

It has also been shown, on an independent sample of Z's decaying into leptons, that the efficiencies for triggering, reconstructing and identifying isolated leptons are very similar in the data and simulations. The residual differences between data and Monte Carlo simulation are corrected via scale factors of the order of a few percent. The same data are used both for signal selection and for the study of the non-top QCD multi-jet and W/Z+jets backgrounds.

Muons are reconstructed using the information from the muon chambers and the silicon tracker [22]. Tracks are required to be of good quality and to be consistent with the reconstructed primary vertex. A kinematic selection of $p_{\mathrm{T}} > 35$ GeV and $|\eta| < 2.1$ is then used to select muon tracks. Electrons are reconstructed using a combination of the shower shape information and track-electromagnetic cluster matching [23]. Special care is taken in order to reject electrons coming from photon conversions. In order to be retained for further analysis, electron candidates are required to have $p_{\mathrm{T}} > 45$ GeV and $|\eta| < 2.5$, excluding the transition region between the barrel and forward calorimeters, $1.4442 < |\eta| < 1.566$, where η is the pseudo-rapidity of the electromagnetic cluster.

Signal events are required to have only one isolated lepton whose origin is consistent with the

reconstructed pp interaction vertex [24]. The leptons are all required to satisfy isolation requirements. The isolation requirements have a twofold use. The first use is a very loose isolation requirement to remove any double-counting between other leptons or jets. For this stage of the selection, muons (electrons) are required to have a relative isolation less than 0.15 (0.2), where the threshold is enlarged in the electron case to allow for the increased amount of radiation close to the track. Here the relative isolation is defined as $I_{\text{rel}} = (I_{\text{charged}} + I_{\text{photon}} + I_{\text{neutral}})/p_{\text{T}}$, where p_{T} is the transverse momentum of the lepton, and I_{charged}, I_{photon} and I_{neutral} are the sums of the transverse energies of the charged particles, the reconstructed photons, and the neutral particles not identified as photons in a cone of size $\Delta R < 0.3$ around the lepton direction, where $\Delta R = \sqrt{\Delta\phi^2 + \Delta\eta^2}$. The energy deposited by the lepton itself does not enter these sums by defining an exclusion cone or $\Delta R < 0.15$ around the lepton direction. Events with more than one loose electron or muon candidate are vetoed. The second use of the isolation requirements is to discriminate events with true prompt W events against those events with leptons from non-prompt sources, and misidentified leptons. Muon events are required to satisfy $I_{\text{rel}} < 0.125$, and electron events are required to satisfy an additional requirement on the detector-based isolation $I_{\text{det}} < 0.05$, where the detector-based isolation is defined as $I_{\text{det}} = (I_{\text{tracking}} + I_{\text{HCAL}} + I_{\text{ECAL}})/p_{\text{T}}$. Here I_{tracking} is the sum of the tracks' transverse momenta, I_{HCAL} and I_{ECAL} are the sums of transverse energy deposits in the hadronic and electromagnetic calorimeters, respectively, within a cone of size $\Delta R < 0.3$ around the lepton direction, excluding the energy deposited by the lepton itself.

Semileptonic $\text{t}\bar{\text{t}}$ events have at least four final state quarks that form jets. These jets are reconstructed using the CMS particle flow algorithm [25] to reconstruct charged and neutral hadrons, photons and leptons, before they are clustered using the anti-k_T jet algorithm [26] with a cone size parameter $\Delta R = 0.5$, as implemented in FastJet version 2.4.2 [27, 28]. Charged hadrons identified as pileup are removed from the inputs to the jet clustering algorithms. The charged hadrons are classified as belonging to a pileup vertex when they are used to reconstruct a vertex that is not the highest p_{T} primary vertex. Muons and electrons that satisfy the (loose) relative isolation requirement (defined above) are excluded from consideration of the jet algorithm. After these corrections, only the neutral component of pileup remains aside from the true jet constituents. The neutral component is removed by applying a residual area-based correction described in Ref. [29, 30]. The mean p_{T} per unit area is computed with the k_{T} algorithm with the "active area" method, with a distance parameter of 0.6, and the jet energy is corrected by the amount of pileup expected in the jet area. The "active area" method adds a large number of infinitely soft "ghost" particles to the clustering sequence to examine into which jet they are clustered, and the area is computed by the set of points for each jet. Due to the different responses in the endcap and barrel calorimeters, η-dependent jet corrections are also applied [31]. The amount of energy expected from underlying event is added back into the jet. The pileup-subtracted jet four momenta are finally corrected for nonlinearities in η and p_{T} with simulated data, with a residual η-dependent correction added to correct for the difference in simulated and true responses [31]. Jet candidates are required to have $p_T > 30$ GeV and $|\eta| < 2.4$.

The neutrino from the leptonic W-decay escapes detection so its presence is inferred from a sizeable transverse energy imbalance in the detector. The missing transverse energy ($\not\!\!E_{\text{T}}$) is defined as the negative of the vector sum of the transverse energies (E_{T}) of all of the particles found by the particle flow algorithm. This is used as an event selection variable in both the muon and electron analyses as a tool to suppress the background from QCD multi-jet events. A cut of $\not\!\!E_{\text{T}} > 20$ (30) GeV is applied in the muon (electron) channel.

Due of the combined effects of the long b-quark lifetime ($\sim$1.5 ps) and the fact that they are

produced with a significant boost, the decays of b-flavored hadrons are quite different from the shorter lived hadronic states. Rather than having an origin consistent with the primary collision vertex, they travel a measurable distance before decaying, resulting in a displaced decay vertex. Thus the origin of the particles from the b-decay is typically inconsistent with the primary vertex position. In the case of a semi-leptonic b-hadron decay, this results in the production of a lepton with a displaced origin, that is also embedded inside a jet. These characteristics can be used to identify b-quark jets and distinguish them from their non-b counterparts. The techniques, known as b-taggers, are used in the analyses presented here to help suppress the backgrounds from W/Z and QCD multi-jet production. This analysis uses a displaced secondary vertex tagger, details of which are given in [5].

4 Cross Section Measurements

The following sections present the measurement procedure and discuss the results obtained from the subset of the data which has at least one b-tagged jet. We present results on the analysis of the muon + jets and electron + jets channel as well as the combined analysis.

4.1 Overview of Fit Procedure

To extract the $t\bar{t}$ cross section we perform a maximum likelihood fit to the number of reconstructed jets ($j = 1$–4, ≥ 5), the number of b-tagged jets ($i = 1, \geq 2$), and the secondary vertex mass distribution in the data. The secondary vertex mass is defined as the mass of the sum of the four-vectors of the tracks associated to the secondary vertex, assuming that each particle has the pion mass. We find this distribution yields a good discrimination between the contributions from light and heavy flavor quark production [7]. We fit the data to the sum of signal and background shapes using a binned Poisson likelihood function.

The templates for the fit are normalized to the expected event yields for 0.8 (1.1) fb^{-1} for the electron+jets (muon+jets) analysis. The four major backgrounds are W+jets, Z+jets, single top quark, and QCD multi-jet production. The templates for the W and Z contributions are normalized such that the NNLO predictions [21] are equal to unity. The W and Z+jets backgrounds come from V+b jets, V+c jets, and V+light flavor events. These three components are allowed to float independently in the fit. During the likelihood maximization, the normalizations of each of these components are extracted. A full detector unfolding is not done, so this is not a meaningful measurement of the W/Z+jets cross section, however the impact of the renormalization and factorization scales on the $t\bar{t}$ cross section is found to be smaller than that predicted by an ad hoc variation of the scales. The single-top background contribution is the sum of the contributions from s and t and tW channels, each normalized to its respective cross section. The QCD multi-jet normalization and the kinematic distribution of the secondary vertex mass are obtained using events in the sideband data regions, and described below.

The shape of the jet multiplicity distribution (N_{jet}) depends on the choice of the jet p_T threshold, and thus is also sensitive to the jet energy scale (JES). In this sense, the fit is intrinsically able to determine the JES from the variations of the N_{jet} distribution as a function of JES. In addition, the jet multiplicity is affected by variation of Q^2 scale. The uncertainty in the b-tag efficiency is also extracted directly from the fit, by using the changes in the relative rates of 1-tag and 2-tag events. A larger b-tag efficiency will result in events moving from 1-tag to 2-tag samples. In contrast, an overall increase in all tag bins together would indicate an increase in the $t\bar{t}$ cross section. Because the JES, the Q^2-scales, and the b-tag efficiency are expected to cause the largest uncertainties on the $t\bar{t}$ cross section measurement, and they are correlated with each

other, they are treated as nuisance parameters in the profile likelihood fit. The combined in-situ measurement of the yields of principal backgrounds and each of these nuisance parameters leads to a significant improvement over analyses which use more conventional techniques for b-tagged cross section measurements.

There are several "nonprompt-W" or "QCD" backgrounds for the muon and electron analyses. The QCD background in the muon + jets channel comes from multi-jet events with heavy flavor decays, kaon and pion decays in flight, and hadronic punch-through in the muon system. Because these are difficult to calculate to the required precision we derive these backgrounds from the data. The normalization is determined by using a comparison of data and simulation in the data sideband region with $\not\!\!E_{\mathrm{T}} < 20$ GeV. The ratio is used to scale the predicted yields for $\not\!\!E_{\mathrm{T}} > 20$ GeV.

While the secondary vertex mass distributions and normalizations of the $\mathrm{t\bar{t}}$, W and Z+jets are modeled by the Monte Carlo simulation, the secondary vertex mass distribution of the contribution due to QCD is derived from the non-isolated ($I_{rel} > 0.2$) data. Because of the correlations between $\not\!\!E_{\mathrm{T}}$ and isolation, the templates for the QCD estimate from the data that are taken from non-isolated samples are modified using the shape taken from the QCD simulation. This treatment is similar in spirit to the QCD treatment in the recent CMS W and Z cross-section measurements [32]. The QCD rate in each jet bin is constrained to the average of the true $\not\!\!E_{\mathrm{T}}$ distribution of the non-isolated region, and the "modified" $\not\!\!E_{\mathrm{T}}$ distribution after accounting for correlations from the Monte Carlo simulation. The QCD component in the fit is constrained to 100 percent of the rate or half the difference between the results, whichever is greater.

The secondary vertex mass shapes for the fit are taken from the non-isolated data. Because of limited statistics, the ≥ 3 jet sample is included as a single template, with separate normalizations for each jet bin.

Similarly, the electron + jets channel is contaminated by photon conversions, jets with a high electromagnetic fraction, and heavy flavor decays. The normalization of this background is also estimated from a fit to the $\not\!\!E_{\mathrm{T}}$ spectrum. However, the non-isolated sidebands do not accurately represent the shape of the $\not\!\!E_{\mathrm{T}}$ distribution. Instead, we rely on multi-jet QCD background shapes obtained from simulation and perform a template fit to the $\not\!\!E_{\mathrm{T}}$ distribution in data in order to determine the normalization with the same $\not\!\!E_{\mathrm{T}}$ procedure as in the muon case. To enhance the statistics, the detector isolation cut is released from 0.05 to 0.15 and looser lepton identification criteria are applied. We verified that the template shapes were unaffected by this procedure. The default method uses a three component fit for W + jets, the electroweak component comprising $\mathrm{t\bar{t}}$ pair production, single top and Z + jets, and the QCD multi-jet background template. The electroweak template is constraint to 30% of the Standard Model expectation whereas all the other templates float freely. As a cross-check we have also studied a four component fit where the $\mathrm{t\bar{t}}$ shape is decoupled from the electroweak template, yielding consistent results. We assign a 100% uncertainty to this template in the joint likelihood fit to determine the cross section.

There are alternative control samples to estimate both the jet energy scale, and the b-tag efficiency. The jet energy scale is measured as described in Section 3. The uncertainty measured is approximately 3% and is used in a Gaussian constraint on the jet energy scale in the likelihood. The b-tag efficiency scale factor is constrained to 1.0 ± 0.1, and the mistag rate scale factor is constrained to 1.0 ± 0.1. The technical implementation of these efficiencies in the likelihood is to weight the tagged jets in the simulation up or down by the data-to-simulation scale factor, and weight untagged jets in the simulation with zero weight.

The number of predicted events with respect to each contribution is given by Equations (1–3), for the $t\bar{t}$ signal and two of the W+jets backgrounds (W+b-jets and W+light flavor). There are similar terms for the other W+jets backgrounds, the single top, and the QCD multi-jet production. Thus, we have

$$N_{t\bar{t}}^{\text{pred}}(i,j) = K_{t\bar{t}} \cdot N_{t\bar{t}}^{\text{MC}}(i,j) \cdot P^{\text{b tag}}(i,j,R_{\text{b tag}}) \cdot P^{\text{mistag}}(i,j,R_{\text{mistag}}) \cdot P^{\text{JES}}(i,j,R_{\text{JES}}) \quad (1)$$

$$N_{Wb\bar{b}}^{\text{pred}}(i,j) = K_{Wb\bar{b}} \cdot N_{Wb\bar{b}}^{\text{MC}}(i,j) \cdot P^{\text{b tag}}(i,j,R_{\text{b tag}}) \cdot P^{\text{mistag}}(i,j,R_{\text{mistag}}) \cdot P^{\text{JES}}(i,j,R_{\text{JES}}) \cdot P^{Q^2}(i,j,R_{Q^2}) \quad (2)$$

$$N_{Wq\bar{q}}^{\text{pred}}(i,j) = K_{Wq\bar{q}} \cdot N_{Wq\bar{q}}^{\text{MC}}(i,j) \cdot P^{\text{mistag}}(i,j,R_{\text{mistag}}) \cdot P^{\text{JES}}(i,j,R_{\text{JES}}) \cdot P^{Q^2}(i,j,R_{Q^2}) \quad (3)$$

where $K_{t\bar{t}}$ is the fitted scale factor for the NLO prediction for $\mathrm{t\bar{t}}$; i and j run over tags and jets, respectively; $K_{Wb\bar{b}}$ is the fitted scale factor for the NNLO prediction for $Wb\bar{b}$ (etc); $N_x^{\text{MC}}(i,j)$ is the number of events expected for sample X, derived from Monte Carlo and corrected with data-to-Monte-Carlo scale factors. The $P^X(i,j,R_X)$ factors are multiplicative functions accounting for the relative differences with respect to the input expected yield, as a function of the assumed value R_X of nuisance parameter X (i.e., b-tag efficiency, jet energy scale, etc). These are interpolated from various configurations in the simulation with polynomials. The convention chosen is that the nominal event yield is at $R_X = 0$ (i.e., no variation in parameter X), and $P(i,j,R_X) = 1.0$ (i.e., multiplicative factor of 1.0 by default). The "$+1\sigma$" variation is at $R_X = 1$, and the "-1σ" variation is at $R_X = -1$.

The fit minimizes the negative log likelihood, summing over the histogram bins (k) of the secondary vertex mass, the number of jets (j), and the number of tags (i). The various constraints (described above) are included as Gaussian penalty terms on the variables, which are represented by C_X. The full profile likelihood expression is

$$-2\ln L = -2\left\{\sum_{i,j}^{\text{tag,jet}}\sum_{k}^{\text{bins}}(\ln\mathcal{P}(N_k^{\text{obs}}(i,j),N_k^{\text{exp}}(i,j))) - \frac{1}{2}\sum_{l}^{\text{constraints}}\frac{(C_X-\hat{C}_X)^2}{\sigma_{C_X}^2}\right\} \quad (4)$$

where $\mathcal{P}$ is a Poisson probability that the predicted yield (N^{exp}, see Equations (1 –3)) given by the various components statistically overlaps with the data (N^{obs}) in each tag/jet bin i,j, given by

$$\ln\mathcal{P}(x,y) = x\ln y - y - \ln\Gamma(x+1) \quad (5)$$

where $\Gamma(x)$ is the Gamma function.

Table 1 shows a summary of all of the inputs to the profile likelihood, as well as the constraints.

There are also a number of systematic uncertainties that are not included directly in the profile likelihood and hence are taken as additional systematic uncertainties outside of the fit result. The largest of these is the systematic uncertainty due to the overall luminosity determination of 4.5%. It has also been shown on independent samples of $Z \to ee$ and $Z \to \mu\mu$ events that the

Table 1: Inputs to the profile likelihood, along with constraints. All values are in percent.

Quantity	Constraint (%)
b-tag Efficiency Scale Factor	100 ± 10
b-tag Mistag Scale Factor	100 ± 10
Jet energy scale relative to nominal	100 ± 3 (η,p_T dependent)
W+jets renormalization/factorization scales	100^{+100}_{-50}
W+jets background normalization	unconstrained
QCD background normalization	100 ± 100
Single-top background normalization	100 ± 30
Z+jets background normalization	100 ± 30

efficiencies for triggering, reconstructing, and identifying isolated leptons of this type are very similar in the data and simulations. We have corrected for the small differences observed. The effect of these uncertainties are not included in the profile likelihood, and hence are taken as an additional systematic uncertainty of 3-3.4%.

There are a number of theoretical uncertainties in the signal modeling that are not included in the profile likelihood. They include differences in the $t\bar{t}$ signal due to renormalization and factorization scales, the amount of initial and final state radiation present, the parton distribution function model, and the matching scale for the matrix-element to parton-shower matching scheme. These are computed from dedicated simulated samples by varying the theoretical parameters of interest according to conservative variations around the reference value. The exception is the parton distribution functions, which are varied by reweighting the sample according to variations in the underlying parton distribution function parameterizations [15]. The numerical impact of each of these is taken as a systematic uncertainty. Specifically, these are 2% for $t\bar{t}$ Q^2 modeling; 2% for initial and final state radiation modeling; 2% for the matrix-element to parton-shower matching in the $t\bar{t}$; and 3.4% for the parton distribution function differences. We also apply 2.5-2.6% due to pileup reweighting;

In all of the cases that are described below, the robustness of the statistical procedure is demonstrated with a priori pseudo-experiments where the expected yields and the parameters in the profile likelihood are sampled randomly according to Poisson or Gaussian statistics (as appropriate). In cases where the true frequentist statistical coverage is not achieved due to the limitations of the profile likelihood method, coverage is assured by correcting for the slight biases (of order 1% in the central values and/or uncertainties).

4.2 Muon + Jets Analysis

The results of the fit in the muon+jets channel are shown in Table 2. The fit considers events with one b-tag (1-tag) and two and more b-tags (2-tag) separately, giving nine jet-tag 'bins' (subsamples) which are fit by the joint likelihood (Equation 4). Table 2 lists the observed and fitted rates for each jet-tag bin.

Table 3 lists the systematic uncertainties from the fit. These include both the theoretical uncertainties from the $t\bar{t}$ modeling and the corrections used to match the simulations to the data and give a total uncertainty of 4.3% for the $t\bar{t}$ signal model. The unclustered energy in the detector results in an additional resolution uncertainty of $<$1% on the $\not\!\!E_{\mathrm{T}}$ scale. We combine these with the data-simulation uncertainties due to the jet energy scale and jet resolution modeling, the b-tag efficiency and mistag rate and obtain a total systematic uncertainty of 7.8%. For illustrative purposes, in Table 3, we have broken up the pieces of the profile likelihood and quote the

Table 2: The fitted number of top and background events in the likelihood fit for muon + jets with least 1 b-tag. Here Wbx, Wcx, and Wqq represent W+b jets, W+c jets, and W+light flavor events, respectively.

	Data	Total Fit	Top	SingleTop	Wbx	Wcx	Wqq	ZJets	QCD
1 Jet 1 Tag	11934	11924.8	419.4	889.9	582.3	7718.9	1486.1	358.5	469.8
2 Jets 1 Tag	7026	7071.6	1479.9	904.5	860.2	2813.4	673.1	223.6	116.9
3 Jets 1 Tag	4067	4015.4	2084.5	408.8	320.5	816.6	213.7	88.1	83.2
4 Jets 1 Tag	1933	1916.0	1395.7	129.2	76.8	187.7	57.7	25.6	43.3
5 Jets 1 Tag	854	878.7	738.1	40.4	21.6	51.6	9.6	11.1	6.3
2 Jets $\geq$ 2 Tags	777	782.5	446.9	153.8	111.4	51.0	8.8	10.6	0.0
3 Jets $\geq$ 2 Tags	1297	1295.4	1053.5	138.6	64.3	28.0	2.0	9.0	0.0
4 Jets $\geq$ 2 Tags	1044	1050.0	955.3	59.3	16.2	15.5	0.9	2.8	0.0
5 Jets $\geq$ 2 Tags	650	642.0	601.1	24.6	9.0	5.6	0.0	1.7	0.0
Total	29582	29576.6	9174.4	2749.0	2062.2	11688.3	2452.0	731.0	719.6

uncertainties due to the individual contributions. These are the result of fixing all of the other parameters of the likelihood and only allowing the chosen term to vary.

Table 3: List of systematic uncertainties for the muon + jet, electron + jet, and combined analyses. Due to the correlation between parameters in the fit, the combined number is not the sum of the squares of the contributions.

Source	Muon Analysis	Electron Analysis	Combined Analysis
Quantity	Uncertainty (%)		
Lepton ID/reco/trigger	3.4	3	3.4
$\not\!\!E_T$ resolution due to unclustered energy	< 1	< 1	< 1
$t\bar{t}$ +jets Q^2 scale	2	2	2
ISR/FSR	2	2	2
ME to PS matching	2	2	2
Pile-up	2.5	2.6	2.6
PDF	3.4	3.4	3.4
Profile Likelihood Parameter	Uncertainty (%)		
Jet energy scale and resolution	4.2	4.2	3.1
b-tag efficiency	3.3	3.4	2.4
W+jets Q^2 scale	0.9	0.8	0.7
Combined	7.8	7.8	7.3

This yields a cross section measurement in the muon + jets channel of

$$\sigma_{t\bar{t}} = 163.2 \pm 3.4(\text{stat.}) \pm 12.7(\text{syst.}) \pm 7.3(\text{lum.}) \text{ pb}. \quad (6)$$

The fit provides in-situ measurements of the scale factors for both b-tagging and the jet energy scale. We obtain a value of 97 ± 1 % for the b-tagging scale factor and a value of 100 ± 2% for the jet energy calibration correction (on top of the standard jet corrections). The scale factors for the W+b-jets and $W + c$-jets components indicate that the contributions in the data may be larger than what is expected by the rescaled predictions. For the W+b-jets component we find a cross section scale-factor of 1.1 ± 0.3 and for the W+c-jets contribution we obtain 1.6 ± 0.1.

4.3 Electron + Jets Analysis

The analysis in the electron channel is performed in the same way as for the muon case. The results are shown in Table 4. The contributions to the systematic uncertainty are summarized in Table 3 .

Table 4: The fitted number of top and background events in the likelihood fit for electron + jets with least 1 b-tag. Here Wbx, Wcx, and Wqq represent W+b jets, W+c jets, and W+light flavor events, respectively.

	Data	Total Pred	Top	SingleTop	Wbx	Wcx	Wqq	ZJets	QCD
1 Jet 1 Tag	6119	6076.6	220.2	314.6	413.7	3789.7	872.1	213.1	253.2
2 Jets 1 Tag	3586	3661.7	764.4	358.0	620.8	1380.3	383.6	152.5	2.2
3 Jets 1 Tag	2142	2120.5	1066.3	187.9	235.2	351.8	97.1	60.2	121.9
4 Jets 1 Tag	1026	1004.9	723.5	65.2	53.0	90.2	35.3	19.4	18.4
5 Jets 1 Tag	475	474.9	386.5	20.1	21.9	21.1	7.8	6.3	11.0
2 Jets $\geq$ 2 Tags	383	373.5	220.0	58.9	60.4	22.9	1.4	9.9	0.1
3 Jets $\geq$ 2 Tags	689	690.7	527.5	58.7	59.6	18.1	0.8	5.7	20.3
4 Jets $\geq$ 2 Tags	553	549.1	485.2	29.3	19.2	3.8	1.1	2.9	7.7
5 Jets $\geq$ 2 Tags	319	329.6	305.7	12.9	6.5	1.1	0.3	1.3	1.8
Total	15292	15281.5	4699.2	1105.6	1490.4	5679.0	1399.5	471.2	436.6

The resulting cross section in the electron + jets channel is

$$\sigma_{\mathrm{t\bar{t}}} = 163.0 \pm 4.4(\mathrm{stat.}) \pm 12.7(\mathrm{syst.}) \pm 7.3(\mathrm{lum.})\ \mathrm{pb}. \quad (7)$$

From the electron channel fit we obtain a result of 97 $\pm$ 2 % for the b-tagging scale factor and 100 $\pm$ 3 % for the jet energy calibration correction (on top of the standard jet corrections). The scale factors for the W+b-jets and $W + c$-jets components are 1.9 $\pm$0.4 and 1.8 $\pm$ 0.1 , respectively. These are in agreement with the results from the muon channel.

4.4 Simultaneous Muon and Electron Channel Analysis

Having established the consistency of the separate channel measurements, we now proceed to perform a combined fit to both channels as the main result of this note. The values in the profile likelihood are assumed to be the same, and the different jet/tag bins are separated according to lepton flavor. To establish our best measurement, we repeat the fit procedure and apply it simultaneously to the data in both the electron and muon channels. We find that the resulting fitted event yields in each tag category are in good agreement with those obtained from the separate channel fits (Tables 2 and 4). Figure 1 shows the comparison of the corresponding observed and fitted vertex mass distributions. Figures 2 and 3 show the data and fit results for the total transverse energy of the event (H_T), the missing transverse energy ($\not\!\!E_{\mathrm{T}}$), and the transverse mass of the W (M_T^W) in the ≥ 3 jets and ≥ 1 tag sample. We find good agreement in all cases.

The correlation matrix for the combined fit is listed in Table 5. The nuisance parameters represent signal and background normalizations, and systematic uncertainties due to Q^2, b-tag efficiency, JES, and mis-tag efficiency (lftag). The corresponding $\mathrm{t\bar{t}}$ cross section measurement is

$$\sigma_{t\bar{t}} = 164.4 \pm 2.8(\text{stat.}) \pm 11.9(\text{syst.}) \pm 7.4(\text{lum.}) \text{ pb} \quad (8)$$

which is in good agreement with both the separate channel measurements and those from the cross-check analysis discussed below. The corresponding summary of the systematic uncertainties is given in Table 3.

The fit provides in-situ measurements of the scale factors for both b-tagging and the jet energy scale. We obtain a result of $97 \pm 1\%$ for the b-tagging scale factor which agrees well with the result obtained in [5]. For the jet energy scale we obtain a result of 99 $\pm 2\%$ in agreement with 1. The scale factors for the W+b-jets and W+c-jets components indicate that the contributions to the data may be larger than what is predicted. For the W+b-jets contribution we find cross section scale-factors of 1.2 ± 0.3 and for the W+c-jets contribution of 1.7 ± 0.1. These results are consistent with the scale factors obtained by the individual lepton flavor analyses.

Table 5: Correlation matrix of the fit to the combined electron and muon data samples with at least one b-tag.

	Top	SingleTop	Wbx	Wcx	Wqq	Zjets	Q^2	btag	JES	lftag
Top	1.000	-0.285	-0.180	0.288	0.032	0.074	-0.135	-0.627	-0.835	0.002
SingleTop	-0.285	1.000	-0.731	0.049	0.047	-0.041	0.069	-0.104	0.134	-0.006
Wbx	-0.180	-0.731	1.000	0.068	0.123	-0.145	0.295	0.195	0.269	-0.002
Wcx	0.288	0.049	0.068	1.000	0.053	0.034	0.673	-0.428	-0.204	-0.011
Wqq	0.032	0.047	0.123	0.053	1.000	-0.139	0.311	-0.058	-0.048	-0.763
ZJets	0.074	-0.041	-0.145	0.034	-0.139	1.000	0.129	0.000	-0.100	0.002
Q^2	-0.135	0.069	0.295	0.673	0.311	0.129	1.000	-0.022	0.231	-0.016
btag	-0.627	-0.104	0.195	-0.428	-0.058	0.000	-0.022	1.000	0.460	-0.011
jes	-0.835	0.134	0.269	-0.204	-0.048	-0.100	0.231	0.460	1.000	0.003
lftag	0.002	-0.006	-0.002	-0.011	-0.763	0.002	-0.016	-0.011	0.003	1.000

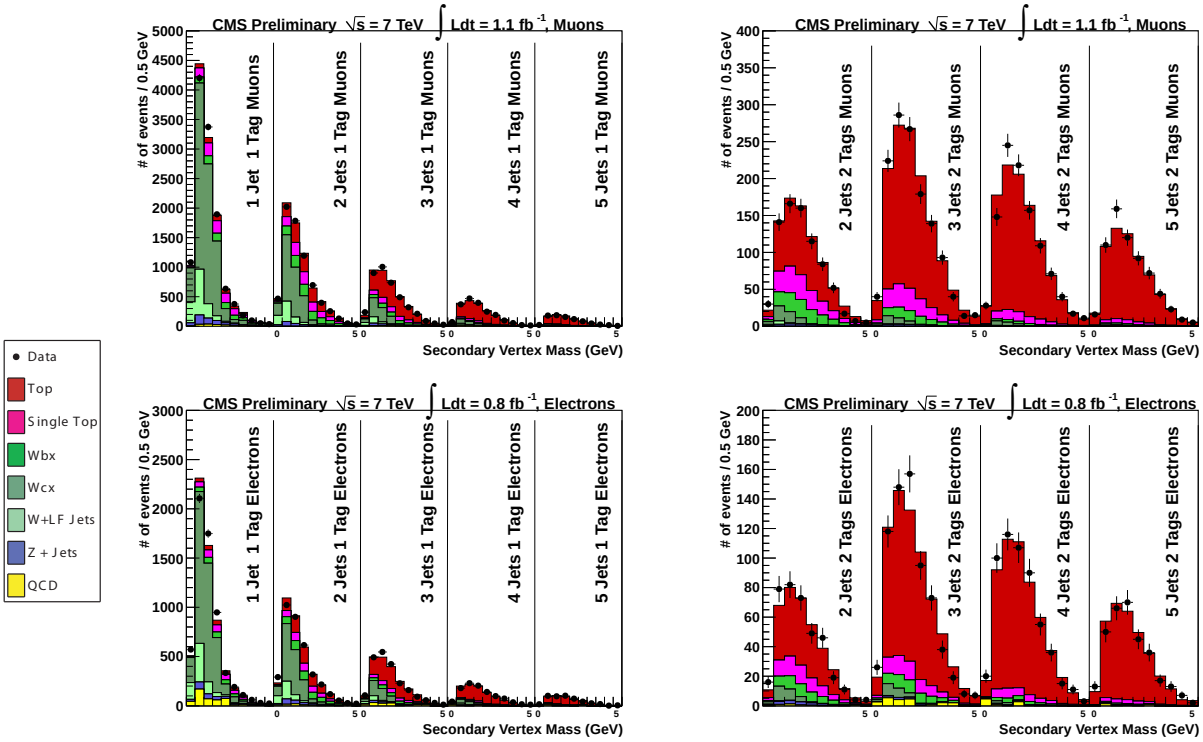

Figure 1: Results of the combined muon and electron channel fit. The top and bottom plots are for the muon and electron channels, respectively. The plots of the left are for single b-tags and those on the right are for $\geq$ 2b-tags. The histograms within each panel correspond to events with 1-, 2-, 3-, 4- and $\geq$5-jets,respectively.

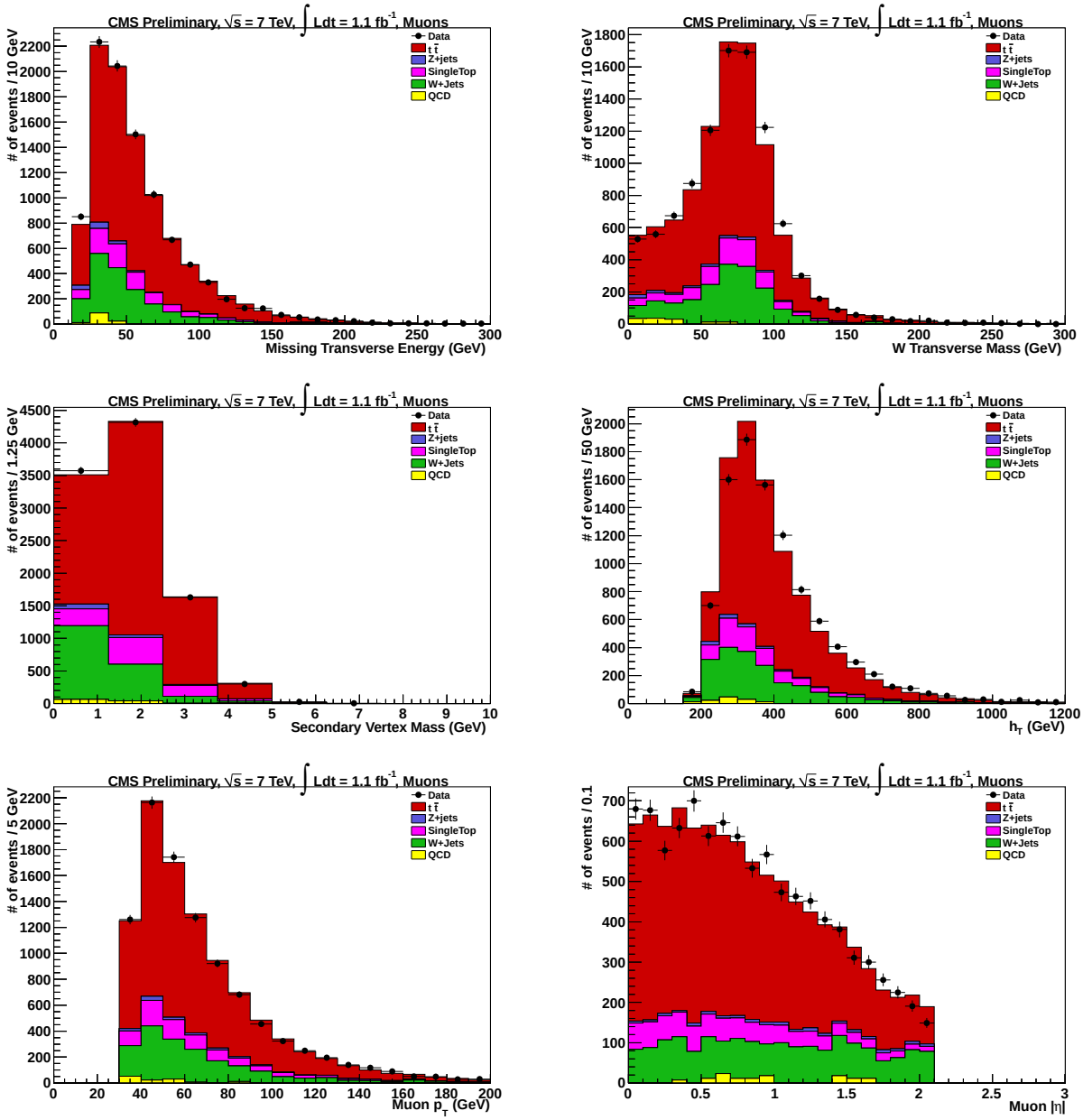

Figure 2: The muon + jets channel's kinematic distributions of the missing transverse energy ($\not\!\!E_{\mathrm{T}}$), the transverse mass of the W (M_T^W), the reconstructed mass of the secondary vertex, the total transverse energy (H_T), the muon transverse momentum, and the η of the muon momentum. These plots are for events containing at least 3 jets and at least 1 tag.

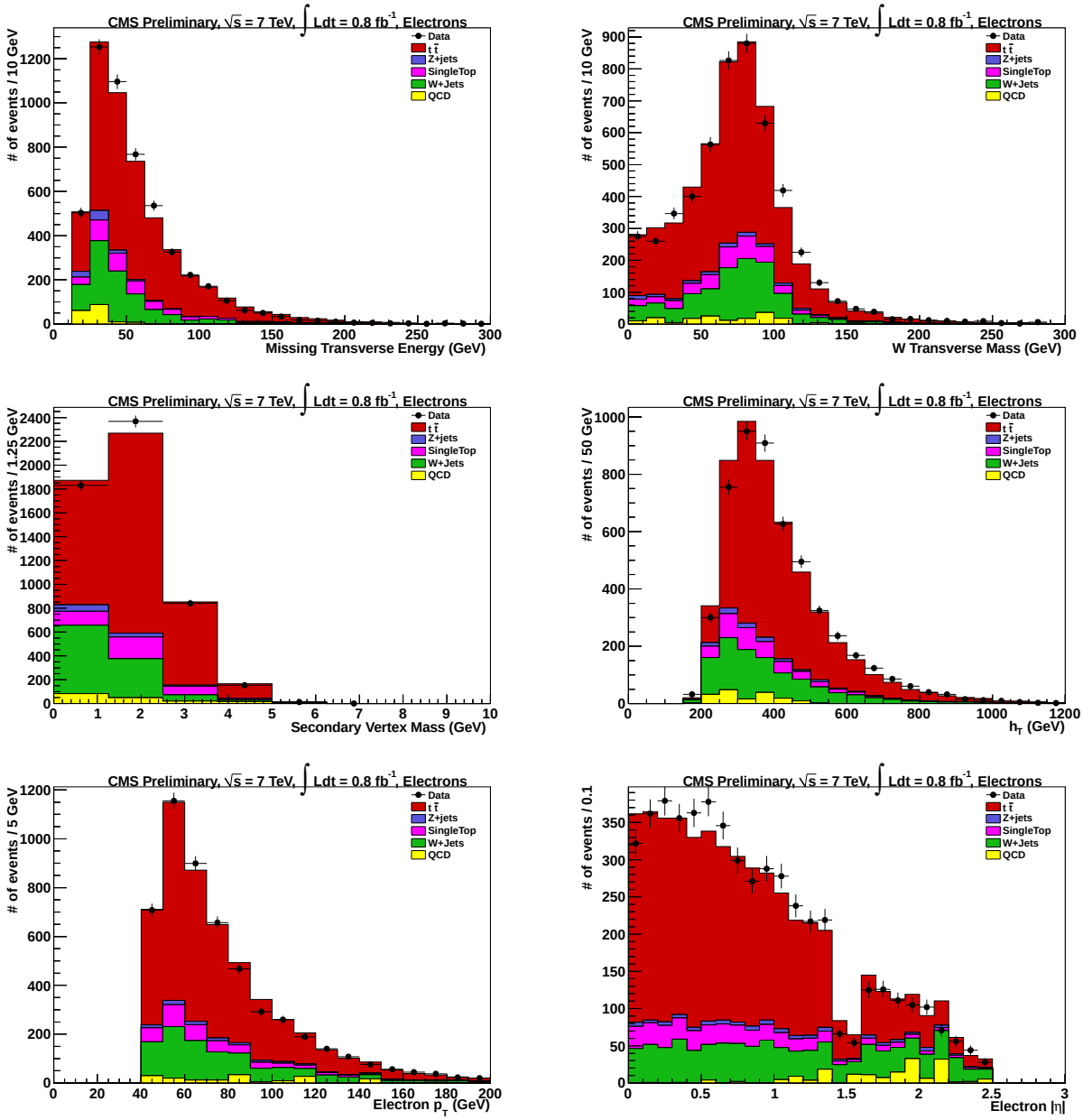

Figure 3: The electron + jets channel's kinematic distributions of the missing transverse energy ($\not\!\!E_{\mathrm{T}}$), the transverse mass of the W (M_T^W), the reconstructed mass of the secondary vertex, the total transverse energy (H_T), the electron transverse momentum, and the η of the electron momentum. These plots are for events containing at least 3 jets and at least 1 tag.

5 Cross check analysis using a combined cross section and b-tag efficiency fit in the muon channel

To cross check the central result described above, we performed an alternative analysis, described in more detail below, which implements essentially the same idea as the reference analysis to determine the $t\bar{t}$ cross section and the b-tagging efficiency in a combined fit, thus improving uncertainties due to their mutual correlation.

The alternative combined $t\bar{t}$ cross section ($\sigma_{t\bar{t}}$) and b-tagging efficiency (ϵ_b) determination uses the μ+jets channel with exactly one b-tag using 1.1 fb^{-1} of data. The analysis is performed in the final state with exactly one muon with a transverse momentum exceeding 35 GeV and at least four jets. The muon and jets are reconstructed and selected in the same way as the reference analysis. In this analysis, no cut on the missing transverse energy ($\not{E}_T$) is applied. To select this topology the event selection requirements of the main analysis are used. The jet associated within the top quark decay with a leptonically decaying W boson is defined as a b-jet as the remaining jet out of four where the three other jets in the event provide the best match to the expected masses of a reconstructed W boson and top quark. The top quark pair cross section is obtained by performing a template fit on the invariant mass distribution of the system built from this b-jet associated to the leptonically decaying top quark and the muon, $m_{\mu j}$.

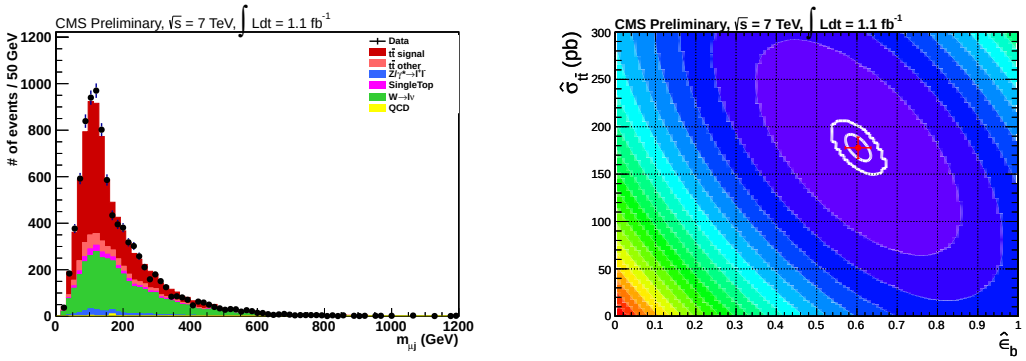

Figure 4: (left) Invariant mass distribution of the b jet candidate and the muon system and (right) $\Delta\chi^2$ distribution in the ($\hat{\epsilon}_b$,$\hat{\sigma}_{t\bar{t}}$) plane.

The $m_{\mu j}$ variable, shown in Figure 4 (left), shows good discriminating power between top quark pair events and background processes. The templates for $t\bar{t}$ and background distributions are obtained from simulation, after applying the reference event selection together with a requirement of medium b-tag on the jet associated to the leptonically decaying top quark, and are fitted on the distribution from data. A b-tag algorithm based on the second highest 2D impact parameter significance among all tracks in the jet [5] is applied with a cut which provides a light-flavor mistagging rate of 1%. This results in a number of observed $t\bar{t}$ events. From this number, using the event selection efficiency and b-tagging efficiency, the cross section is obtained. The b-tagging efficiency that enters the cross section calculation is measured simultaneously with the $t\bar{t}$ cross section. The b-tagging efficiency is determined by reconstructing the b tag discriminant distribution for true b jets ($\hat{\Delta}_b$) in a fully data-driven way.

Before applying the b-tagging criteria on the b-jet associated to the leptonically decaying top quark in the events, these candidates for b-flavored jets are used to define a b candidate jet sample. This jet sample is divided into a b-flavor enriched and b-flavor depleted subsample. This subdivision is performed according to the $m_{\mu j}$ variable of the event, which yields the b enriched region as 80 GeV$< m_{\mu j} <$ 150 GeV and the b depleted region as 150 GeV$< m_{\mu j} <$ 250

GeV. The subdivision is defined such that the $m_{\mu j}$ variable remains uncorrelated with the b-tagging discriminators in the selected enriched and depleted regions.

To obtain the true b-jet discriminator ($\hat{\Delta}_b$), the non-b jet contamination in the b flavor enriched subsample is removed by subtracting the b-tag discriminant distribution of the b-flavor depleted subsample (Δ_b^{depl}) from the b-flavor enriched subsample (Δ_b^{enr}).

$$\hat{\Delta}_b = \Delta_b^{enr} - F \times \Delta_b^{depl} \tag{9}$$

The factor F in Equation (9) represents the ratio between the number of non-b jets in the b-flavor enriched and b-flavor depleted subsamples which therefore rescales the number of non-b jets in the depleted region to the number of non-b jets in the enriched subsample. This factor F is obtained by constructing a control sample with a high purity in non-b jets. The control sample of jets is defined as those jets in the events which are associated with the hadronically decaying W boson. Additionally these jets in the control sample are requested to be anti-b-tagged to further reduce the b jet contamination. In the control sample, the same subsamples are defined as within the signal b candidate jet sample by use of the $m_{\mu j}$ variable which allows direct access to the factor F from data. The kinematics of the jets in the control sample are matched to those in the signal b candidate sample using reweighing techniques based on the observed data itself . Also in the data driven determination of F and in the application of Equation (9) the participating jets in the b-flavor depleted region are reweighed to match the kinematics of the jets in the b-flavor enriched region. From the estimated b-tag discriminator distribution, $\hat{\Delta}_b$, the b-tagging efficiency for diverse working points is estimated.

For a measured b-tagging efficiency of 60.3 $\pm$ 3.2 (stat.) $\pm$ 33.1 (syst.)% for the tagger and working point defined above, a $\mathrm{t\bar{t}}$ cross-section of 177.8 $\pm$ 11.2 (stat.) $\pm$ 50.6 (syst.) $\pm$ 11.3 (lumi.) pb is measured. This is in a good agreement with the reference analysis result. Figure 4 (right) shows the correlation between the b tagging efficiency and the cross section from data.

The dominating systematic uncertainty in both measurements arises from the uncertainty in the determination of the jet energy scale.

6 Summary

We have presented an update of an analysis [7] of the $\mathrm{t\bar{t}}$ production cross section at $\sqrt{s} = 7$ TeV using the CMS detector operating at the LHC during 2011. The data analyzed corresponds to a luminosity of 0.8 (1.1) pb^{-1} of electron (muon) + jets data, using b-tagging to suppress the backgrounds. We measure the $\mathrm{t\bar{t}}$ cross sections with a profile likelihood method using a fit to the number of reconstructed jets, the number of b-tagged jets, and the secondary vertex mass distribution in the individual electron and muon channels:

μ+jets:

$$\sigma_{\mathrm{t\bar{t}}} = 163.2 \pm 3.4(\mathrm{stat.}) \pm 12.7(\mathrm{syst.}) \pm 7.3(\mathrm{lum.})\ \mathrm{pb} \tag{10}$$

e+jets:

$$\sigma_{\mathrm{t\bar{t}}} = 163.0 \pm 4.4(\mathrm{stat.}) \pm 12.7(\mathrm{syst.}) \pm 7.3(\mathrm{lum.})\ \mathrm{pb} \tag{11}$$

and from the combined analysis of both channels we obtain a result of

$$\sigma_{t\bar{t}} = 164.4 \pm 2.8(\text{stat.}) \pm 11.9(\text{syst}) \pm 7.4(\text{lum.})\ \text{pb} \quad (12)$$

This is the most precise measurement of $t\bar{t}$ production cross section at CMS. This result is in good agreement with the QCD predictions of 164^{+6}_{-10} pb [33], [34], 163^{+11}_{-10} pb [35] and $149 \pm 11\,pb$ [36] that are based on the full NLO matrix elements and the resummation of the leading and next-to-leading soft logarithms. We also present a cross check analysis which agrees with these results.

References

[1] CDF Collaboration, "Observation of top quark production in $\bar{p}p$ collisions", *Phys. Rev. Lett.* **74** (1995) 2626, arXiv:hep-ex/9503002. doi:10.1103/PhysRevLett.74.2626.

[2] D0 Collaboration, "Observation of the top quark", *Phys. Rev. Lett.* **74** (1995) 2632, arXiv:hep-ex/9503003. doi:10.1103/PhysRevLett.74.2632.

[3] J. R. Incandela et al., "Status and Prospects of Top-Quark Physics", *Prog. Part. Nucl. Phys.* **63** (2009) 239, arXiv:0904.2499. doi:10.1016/j.ppnp.2009.08.001.

[4] L. Evans and P. Bryant (editors), "LHC Machine", *JINST* **3** (2008) S08001. doi:10.1088/1748-0221/3/08/S08001.

[5] CMS Collaboration, "Performance of b-jet identification in CMS", *CMS Physics Analysis Summary* **CMS-PAS-BTV-11-001** (2011).

[6] CMS Collaboration, "Measurement of CMS Luminosity", *CMS Physics Analysis Summary* **CMS-PAS-EWK-10-004** (2010).

[7] CMS Collaboration, "Measurement of the $t\bar{t}$ production cross section in pp collisions at 7 TeV in lepton+jets events using b-quark jet identification", arXiv:hep-ex/1108.3773. Submitted to *Phys. Rev. D*.

[8] J. Alwall et al., "MadGraph/MadEvent v4: The New Web Generation", *JHEP* **09** (2007) 028, arXiv:0706.2334. doi:10.1088/1126-6708/2007/09/028.

[9] T. Sjostrand, S. Mrenna, and P. Z. Skands, "PYTHIA 6.4 Physics and Manual", *JHEP* **05** (2006) 026, arXiv:hep-ph/0603175. doi:10.1088/1126-6708/2006/05/026.

[10] J. Allison et al., "Geant4 developments and applications", *IEEE Trans. Nucl. Sci.* **53** (2006) 270. doi:10.1109/TNS.2006.869826.

[11] J. Campbell and R. Ellis, "MCFM for the Tevatron and the LHC", *FERMILAB-Conf-10-244-T* (2010) 205–206, arXiv:hep-ph/1007.3492.

[12] A. D. Martin, W. J. Stirling, R. S. Thorne et al., "Uncertainties on α_s in global PDF analyses and implications for predicted hadronic cross sections", *Eur. Phys. J.* **C64** (2009) 653–680, arXiv:0905.3531. doi:10.1140/epjc/s10052-009-1164-2.

[13] H.-L. Lai et al., "Uncertainty induced by QCD coupling in the CTEQ-TEA global analysis of parton distributions", arXiv:1004.4624.

[14] F. Demartin, S. Forte, E. Mariani et al., "The impact of PDF and α_s uncertainties on Higgs Production in gluon fusion at hadron colliders", *Phys. Rev.* **D82** (2010) 014002, arXiv:1004.0962. doi:10.1103/PhysRevD.82.014002.

[15] . http://www.hep.ucl.ac.uk/pdf4lhc/.

[16] J. M. Campbell, R. Frederix, F. Maltoni et al., "Next-to-Leading-Order Predictions for t-Channel Single-Top Production at Hadron Colliders", *Phys. Rev. Lett.* **102** (2009) 182003, arXiv:0903.0005. doi:10.1103/PhysRevLett.102.182003.

[17] J. M. Campbell and F. Tramontano, "Next-to-leading order corrections to W t production and decay", *Nucl. Phys.* **B726** (2005) 109–130, arXiv:hep-ph/0506289. doi:10.1016/j.nuclphysb.2005.08.015.

[18] J. M. Campbell, R. K. Ellis, and F. Tramontano, "Single top production and decay at next-to-leading order", *Phys. Rev.* **D70** (2004) 094012, arXiv:hep-ph/0408158. doi:10.1103/PhysRevD.70.094012.

[19] N. Kidonakis, "Two-loop soft anomalous dimensions for single top quark associated production with a W^- or H^- ", *Phys.Rev.* **D82** (2010) 054018, arXiv:1005.4451. doi:10.1103/PhysRevD.82.054018.

[20] N. Kidonakis, "Next-to-next-to-leading logarithm resummation for *s*-channel single top quark production", *Phys. Rev. D* **81** (Mar, 2010) 054028. doi:10.1103/PhysRevD.81.054028.

[21] K. Melnikov and F. Petriello, "Electroweak gauge boson production at hadron colliders through O(alpha(s)**2)", *Phys. Rev.* **D74** (2006) 114017, arXiv:hep-ph/0609070. doi:10.1103/PhysRevD.74.114017.

[22] CMS Collaboration, "Performance of muon identification in pp collisions at $\sqrt{s}$ = 7 TeV", *CMS Physics Analysis Summary* **CMS-PAS-MUO-10-002** (2010).

[23] CMS Collaboration, "Electron reconstruction and identification at $\sqrt{s}$=7 TeV", *CMS Physics Analysis Summary* **CMS-PAS-EGM-10-004** (2010).

[24] CMS Collaboration, "CMS Tracking Performance Results from Early LHC Operation", *CMS Physics Analysis Summary* **CMS-PAS-TRK-10-001** (2010) arXiv:1007.1988.

[25] CMS Collaboration, "Commissioning of the Particle-Flow Reconstruction in Minimum-Bias and Jet Events from pp Collisions at 7 TeV", *CMS PAS* **PFT-10-002** (2010).

[26] M. Cacciari, G. P. Salam, and G. Soyez, "The anti-kt jet clustering algorithm", *JHEP* **04** (2008) 063, arXiv:0802.1189.

[27] M. Cacciari and G. P. Salam, "Dispelling the N**3 myth for the k(t) jet-finder", *Phys. Lett.* **B641** (2006) 57–61, arXiv:hep-ph/0512210. doi:10.1016/j.physletb.2006.08.037.

[28] M. Cacciari, G. P. Salam, and G. Soyez, "fastjet Package",. http://fastjet.fr/.

[29] M. Cacciari, G. P. Salam, and G. Soyez, "The Catchment Area of Jets", *JHEP* **04** (2008) 005, arXiv:0802.1188. doi:10.1088/1126-6708/2008/04/005.

[30] M. Cacciari and G. P. Salam, "Pileup subtraction using jet areas", *Phys. Lett.* **B659** (2008) 119–126, arXiv:0707.1378. doi:10.1016/j.physletb.2007.09.077.

[31] CMS Collaboration, "Jet Energy Corrections determination at 7 TeV", *CMS PAS JME-10-010* (2010).

[32] CMS Collaboration, "Measurements of Inclusive W and Z Cross Sections in pp Collisions at $\sqrt{s} = 7$ TeV", *Journal of High Energy Physics* **2011** (2011) 1–40, arXiv:1012.2466. doi:10.1007/JHEP01(2011)080.

[33] M. Aliev, H. Lacker, U. Langenfeld et al., "HATHOR: HAdronic Top and Heavy quarks crOss section calculatoR", *Comput.Phys.Commun.* **182** (2011) 1034–1046, arXiv:1007.1327. doi:10.1016/j.cpc.2010.12.040.

[34] U. Langenfeld, S. Moch, and P. Uwer, "Measuring the running top-quark mass", *Phys.Rev.* **D80** (2009) 054009, arXiv:0906.5273. doi:10.1103/PhysRevD.80.054009.

[35] N. Kidonakis, "Next-to-next-to-leading soft-gluon corrections for the top quark cross section and transverse momentum distribution", *Phys.Rev.* **D82** (2010) 114030, arXiv:1009.4935. doi:10.1103/PhysRevD.82.114030.

[36] V. Ahrens, A. Ferroglia, M. Neubert et al., "Renormalization-Group Improved Predictions for Top-Quark Pair Production at Hadron Colliders", *JHEP* **1009** (2010) 097, arXiv:1003.5827.